Angewandte Chemie
Eine Zeitschrift der Gesellschaft Deutscher Chemiker

Supporting Information

69451 Weinheim, Germany

A Heterometallic Fe^{II}–Dy^{III} Single-Molecule Magnet with a Record Anisotropy Barrier**

Jun-Liang Liu, Jie-Yi Wu, Yan-Cong Chen, Valeriu Mereacre, Annie K. Powell, Liviu Ungur,* Liviu F. Chibotaru, Xiao-Ming Chen, and Ming-Liang Tong**

anie_201407799_sm_miscellaneous_information.pdf

Contents of the Supporting Information

1. Synthetic Procedures and Experimental Techniques

Experimental Section

General Remarks:

All chemicals were commercially available and used as received without further purification. The C, H, and N microanalyses were carried out with an Elementar Vario-EL CHNS elemental analyzer. The FT-IR spectra were recorded from KBr pellets in the range 4000-400 cm^{-1} on an EQUINOX 55 spectrometer.

Synthesis of $[Fe_2Dy(L)_2(H_2O)]ClO_4{\cdot}2H_2O$ (2) and $[Fe_2Y(L)_2(H_2O)]ClO_4{\cdot}2H_2O$ (3)

All procedures were conducted under an inert N_2 atmosphere by using Schlenk techniques. 5-chloro-salicylaldehyde (0.6 mmol, 97 mg) was mixed with tris(2-aminoethy1)amine (0.2 mmol, 30 mg) in 25 mL methanol. The resulting yellow solution was stirred for 5 min, and then added $NaBH_4$ (~30 mg) until the solution vanished to colorless. After that, it was bubbling nitrogen for additional 30 min. The oxygen-free solution was added to the mixture of $Dy(NO_3)_3{\cdot}6H_2O$ (0.1 mmol, 46 mg) and $Fe(ClO_4)_2{\cdot}xH_2O$ (52 mg), and then the triethylamine (~75 µL) was dropwise added to the solution. After stirring for 1 min and then slowly aerating the nitrogen for 3 h, ~30 mg (~20 % yield based on 5-chloro-salicylaldehyde) light-pink crystals were obtained in the remaining red solution (~5 mL).

In a procedure analogous to that described above for $[Fe_2Dy]$, $[Fe_2Y]$ was synthesized by the reaction of $Y(NO_3)_3{\cdot}6H_2O$.

Anal. Calc. (%) for **2**: N, 7.19; C, 41.64; H, 4.27; Found (%) for **2**: N, 7.05; C, 41.86; H, 4.46. IR data (KBr, cm^{-1}) for **2**: 3423s, 3257s, 2976m, 2937m, 2758w, 2738w, 2679m, 1591s, 1473vs, 1385vs, 1309s, 1281s, 1144s, 1113s, 1088s, 958m, 941m, 881m, 823s, 781m, 748m, 679s, 627vs, 519m.

Anal. Calc. (%) for **3**: N, 7.55; C, 43.71; H, 4.48; Found (%) for **3**: N, 7.49; C, 43.55; H, 4.39. IR data (KBr, cm^{-1}) for **3**: 3423s, 3257s, 2974m, 2929m, 2765w, 2738w, 2679m, 1591s, 1473vs, 1385vs, 1311s, 1279s, 1144s, 1119s, 1086s, 959m, 953m, 883m, 823s, 781m, 752m, 671s, 627vs, 519m.

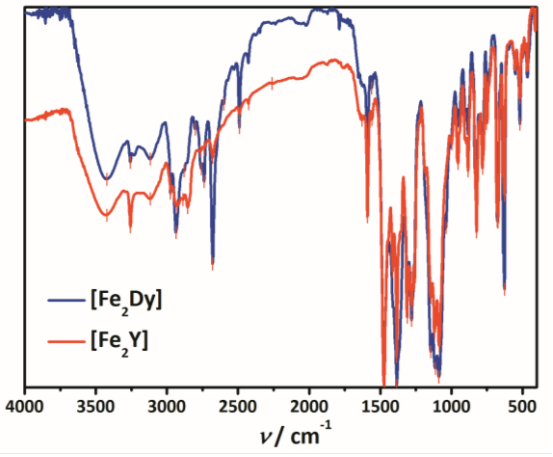

Figure S1.1. Infra-red spectra for **2** and **3**.

X-ray Crystallographic Study

Diffraction intensities were collected on a Rigaku R-AXIS SPIDE IP diffractometer with MoK_α radiation (λ= 0.71073 Å) and an Oxford Diffraction Gemini R CCD diffractometer with CuK_α radiation (λ = 1.54178 Å) for **2** and **3** at 150 K, respectively. The structures were solved by direct methods, and all non-hydrogen atoms were

refined anisotropically by least-squares on F^2 using the SHELXTL program. Anisotropic thermal parameters were assigned to all non-hydrogen atoms. Hydrogen atoms on organic ligands were generated by the riding mode.[1] CCDC reference numbers 978429 (**2**) and 978430 (**3**).

Magnetic measurements

Magnetic susceptibility measurements were performed with a Quantum Design MPMS-XL7 SQUID. Polycrystalline samples were embedded in vaseline to prevent torqueing. Data were corrected for the diamagnetic contribution calculated from Pascal constants.

[1] a) G. M. Sheldrick, *Acta Crystallogr*. **2008**, *A64*, 112; b) G. M. Sheldrick, *SHELXTL 6.10*, Bruker Analytical Instrumentation, Madison, Wisconsin, USA, **2000**.

Structure and Crystallographic Data

Table S2.1. Crystallographic Data and Structural Refinements for 2 and 3.

Compound	**2**	**3**
Molecular formula	$DyFe_2Cl_7O_{13}N_8C_{54}H_{66}$	$YFe_2Cl_7O_{13}N_8C_{54}H_{66}$
Formula weight	1557.50	1483.91
Temperature / K	150	150
Radiation type	MoK_α	CuK_α
Crystal system	Orthorhombic	Orthorhombic
Space group	*Pbca*	*Pbca*
a / Å	21.9280(11)	21.9285(3)
b / Å	15.7064(8)	15.6773(2)
c / Å	36.8044(17)	36.6317(5)
V / Å^3	12675.8(11)	12593.2(3)
Z	8	8
D_{calcd} / g cm^{-3}	1.632	1.565
GOF	1.025	1.034
R_1 [$I \geq 2\sigma(I)$]$^{a)}$	0.0619	0.0541
wR_2(all data)$^{b)}$	0.1695	0.1429

$^{a)}R_1 = \sum||F_o|-|F_c||/\sum|F_o|$, $^{b)}wR_2 = [\sum w(F_o^2-F_c^2)^2/\sum w(F_o^2)^2]^{1/2}$

Table S2.2. Selected bond lengths [Å] for 2 and 3.

	2			**3**	
Dy1	Dy1—O1	2.193(5)	**Y1**	Y1—O1	2.178(3)
	Dy1—O2	2.378(5)		Y1—O2	2.467(5)
	Dy1—O3	2.380(5)		Y1—O3	2.363(3)
	Dy1—O4	2.190(5)		Y1—O4	2.188(3)
	Dy1—O5	2.387(5)		Y1—O5	2.363(3)
	Dy1—O6	2.324(4)		Y1—O6	2.315(3)
	Dy1—O1w	2.492(7)		Y1—O1w	2.467(5)
Fe1	Fe1—O2	2.147(6)	**Fe1**	Fe1—O2	2.141(4)
	Fe1—O3	2.040(5)		Fe1—O3	2.041(3)
	Fe1—N1	2.237(7)		Fe1—N1	2.241(5)
	Fe1—N2	2.255(6)		Fe1—N2	2.263(5)
	Fe1—N3	2.224(7)		Fe1—N3	2.206(5)
	Fe1—N4	2.176(7)		Fe1—N4	2.174(4)
Fe2	Fe2—O5	2.063(5)	**Fe2**	Fe2—O5	2.059(3)
	Fe2—O6	2.245(6)		Fe2—O6	2.235(3)
	Fe2—N5	2.338(7)		Fe2—N5	2.335(5)
	Fe2—N6	2.202(7)		Fe2—N6	2.189(5)
	Fe2—N7	2.214(7)		Fe2—N7	2.208(4)
	Fe2—N8	2.185(7)		Fe2—N8	2.186(4)

Table S2.3. The CShM values calculated by *SHAPE* 2.1 for 2 and 3.

	CN	**Coordination Geometry**	**2**	**3**
Dy^{III} / Y^{III}	**7**	**pentagonal bipyramid (D_{5h})**	Dy1: 0.692	Y1: 0.664
		capped trigonal prism (C_{2v})	Dy1: 4.905	Y1: 4.965
Fe^{II}	**6**	**octahedron (O_h)**	Fe1: 3.456 Fe2: 7.473	Fe1: 3.466 Fe2: 7.559
		trigonal prism (D_{3h})	Fe1: 8.426 Fe2: 6.316	Fe1: 8.423 Fe2: 6.227

2. Plots of Magnetic Data

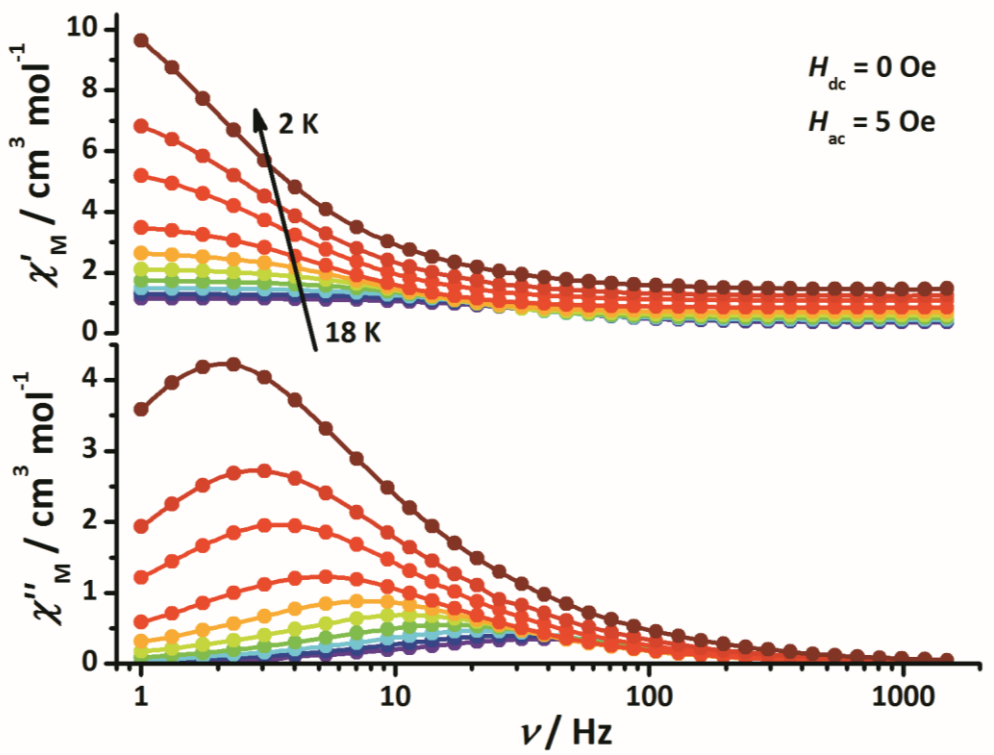

Figure S3.1. Plots of ac susceptibility *vs.* frequency at H_{ac} = 5 Oe, H_{dc} = 0 Oe, oscillating at 1–1488 Hz for **2** in the temperature range of 2−18 K.

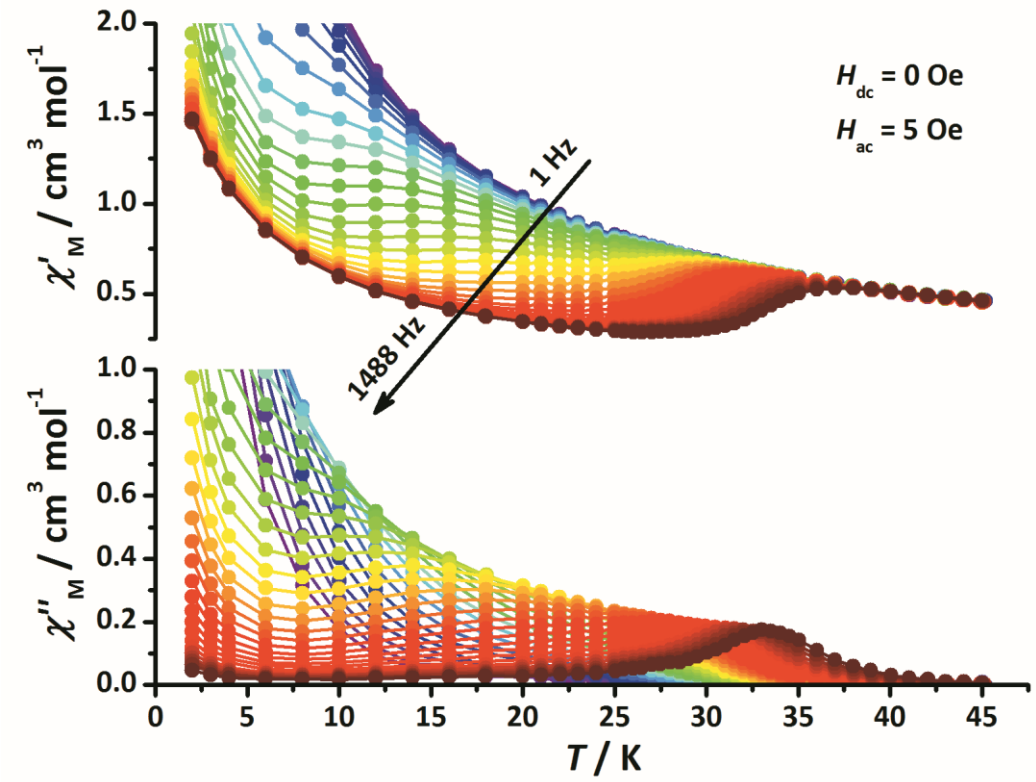

Figure S3.2. Plots of ac susceptibility *vs.* temperature at H_{ac} = 5 Oe, H_{dc} = 0 Oe, oscillating at 1–1488 Hz for **2** in the temperature range of 2−45 K.

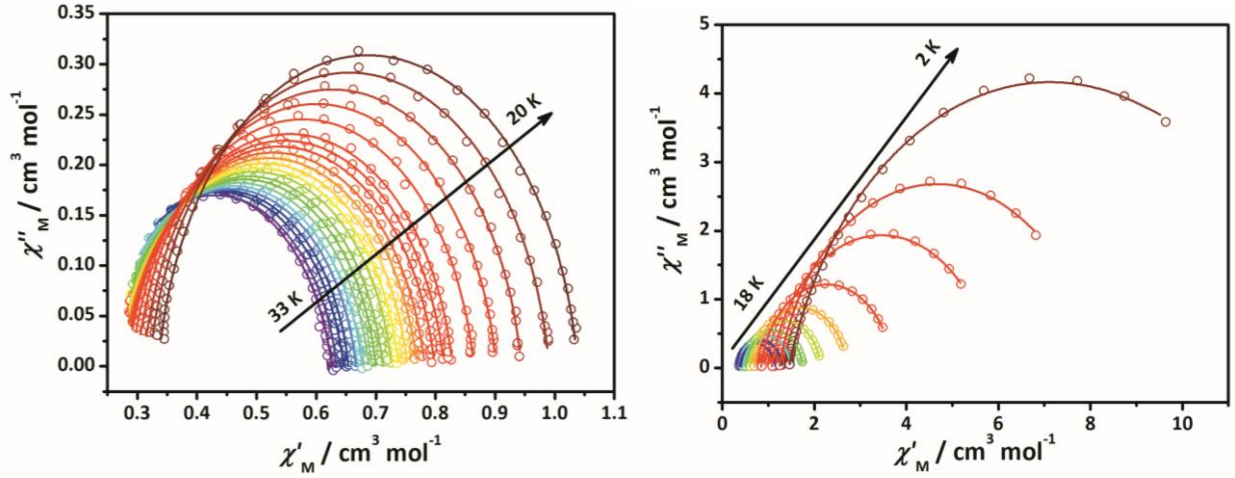

Figure S3.3. Cole-Cole plots in the temperature range of 20−33 K (*left*) and 2−18 K (*right*) for **2**. The solid lines represent the best fitting of the experimental data to the generalized Debye model.

3. Plots of Mössbauer spectra

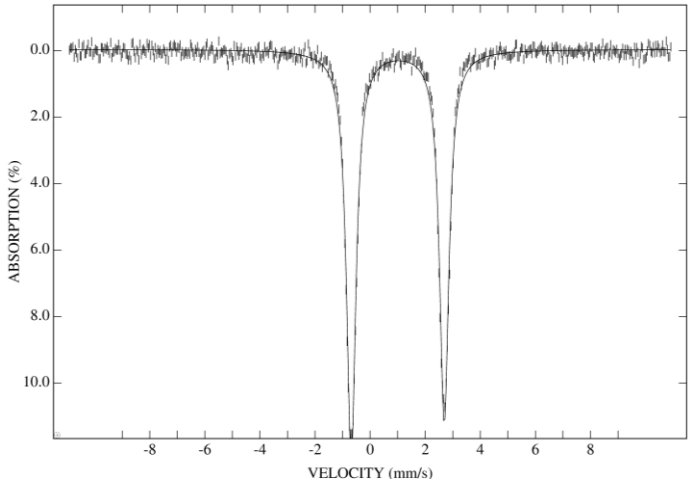

Figure S4.1. Mössbauer spectrum of [$Fe^{II}_2Y^{III}$] at 3 K in a weak applied magnetic field of 300 G. The solid lines are Lorentz fits to the data.

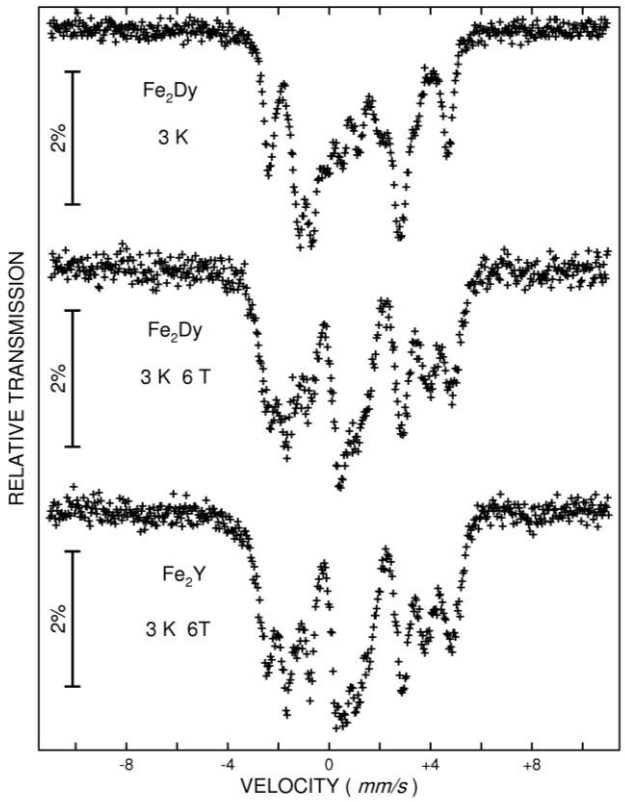

Figure **S4.2.** Mössbauer spectra of [$Fe^{II}_2Dy^{III}$] (3 K, 0 T), [$Fe^{II}_2Dy^{III}$] (3 K, 6 T) and [$Fe^{II}_2Y^{III}$] (3 K, 6 T).

4. Ab initio Calculations for 2

All calculations on individual magnetic centers were done with MOLCAS 7.8 and are of CASSCF/RASSI/SINGLE_ANISO type.
For Dy^{3+}: Active space of the CASSCF included 9 electrons in seven 4f orbitals of the Dy^{3+}.
The spin-orbit coupling included the mixing of 21 sextets, 128 quartets and 130 doublet states.
For Fe^{2+}: Active space of the CASSCF included 6 electrons in 10 (3d + 3d') orbitals of the Fe^{2+}. 3d' shell was added to account for the "double shell" effect. The spin-orbit coupling included the mixing of 5 spin quintets, 45 spin triplets and 50 spin doublet states (all states arising from the various electron populations of the $3d^6$ configuration).

When the Dy ion was computed, the neighbouring Fe ions were computationally replaced by diamagnetic Zn. When Fe ions were computed, the Dy ion was computationally replaced by diamagnetic Lu. The fragments employed for Fe were slightly reduced.

Table S5.1: Contractions of the employed ANO-RCC basis sets.

Basis 1	Basis 2
Dy.ANO-RCC...7s6p4d3f1g.	Dy.ANO-RCC...8s7p5d4f2g1h.
Zn.ANO-RCC...5s4p2d1f.	Lu.ANO-RCC...7s6p4d2f1g.
O.ANO-RCC...3s2p1d.	Zn.ANO-RCC...6s5p3d2f1g.
N.ANO-RCC...3s2p.	O.ANO-RCC...4s3p2d1f.
C.ANO-RCC...3s2p.	N.ANO-RCC...3s2p.
H.ANO-RCC...2s.	C.ANO-RCC...3s2p.
	H.ANO-RCC...2s.

Table S5.2: Energies of the lowest Kramers doublets (cm^{-1}) on the Dy fragment.

Kramers doublets (cm^{-1})	
Basis 1	Basis 2
0.000	0.000
279.487	313.941
307.204	320.848
395.425	430.119
457.531	485.355
499.686	529.417
580.312	610.859
609.051	639.496
3705.093	3711.297
3830.607	3848.518
3873.803	3905.158
3915.307	3942.424
3970.305	3997.421
4036.942	4064.371
4092.321	4122.544
6318.075	6336.497
6343.908	6356.097
6391.557	6413.382
6446.234	6473.249
6516.270	6543.809
6602.450	6632.929
8278.727	8298.386
8314.581	8328.548
8362.798	8383.456
8442.011	8468.355
8531.182	8560.507
9815.617	9834.480
9847.289	9861.342
9948.233	9971.844
10048.897	10077.013
...	...

Table S5.3: Energies (cm^{-1}) and *g* tensors of the lowest Kramers doublets (KD) on the Dy fragment.

KD		Basis 1		Basis 2	
		E	*g*	*E*	*g*
1	g_X	0.000	0.00001	0.000	0.00001
	g_Y		0.00002		0.00002
	g_Z		19.85681		19.85862
2	g_X	279.487	0.16465	313.941	0.53066
	g_Y		0.23521		3.39562
	g_Z		19.37465		14.58605
3	g_X	307.204	0.05636	320.848	0.57555
	g_Y		0.33799		3.29900
	g_Z		16.56609		12.38076
4	g_X	395.425	1.14366	430.119	1.48528
	g_Y		1.91047		2.05378
	g_Z		15.74018		15.69166
5	g_X	457.531	8.56105	485.355	8.33896
	g_Y		7.10653		7.34423
	g_Z		5.51079		5.36208
6	g_X	499.686	1.00607	529.417	1.02470
	g_Y		1.72513		2.06245
	g_Z		13.35737		13.24745
7	g_X	580.312	0.34207	610.859	0.14119
	g_Y		1.45575		1.58780
	g_Z		15.87776		15.92409
8	g_X	609.051	0.56943	639.496	0.59032
	g_Y		1.40872		1.24548
	g_Z		18.15522		18.23591

Table S5.4: Angles between the main magnetic axes of the lowest Kramers doublet obtained in different computational approximations (degrees).

	Basis 1	Basis 2
Basis 1	0.000	0.278
Basis 2	0.278	0.000

Table S5.5: Angles between the main magnetic axes of the lowest Kramers doublet and the two shortest DyO bonds (with oxygens O1 and O4 in the structure file).

	Basis 1	Basis 2
O1	4.710	4.717
O4	5.472	5.381

Table S5.6: Energies of the lowest spin-orbit states (cm^{-1}) on the Fe fragments (Fe1 and Fe2).

Fe1		Fe2	
Basis 1	Basis 2	Basis 1	Basis 2
0.000	0.000	0.000	0.000
2.613	2.740	2.675	3.152
16.352	16.552	10.021	8.454
33.464	34.276	24.008	22.641
35.123	35.882	24.403	22.936
933.644	905.183	598.146	590.453
936.529	908.225	599.928	592.551
973.846	946.690	627.712	618.880
998.964	973.371	643.274	636.089
1007.004	981.745	649.497	641.733
1575.382	1503.461	1978.861	1960.394
1577.754	1506.267	1980.493	1962.013
1613.002	1542.350	2005.888	1987.527
1631.474	1562.695	2019.763	2001.364
1638.417	1569.518	2024.885	2006.519
9019.903	8931.357	7703.952	7625.188
9020.042	8931.493	7704.031	7625.252
9023.553	8935.198	7719.305	7641.073

9025.167	8936.825	7721.779	7643.393
9025.919	8937.635	7726.171	7648.014
11133.329	10977.517	8918.301	8783.239
11134.058	10978.301	8921.750	8786.779
11135.018	10979.266	8923.731	8788.963
11137.933	10982.360	8935.617	8801.263
11138.017	10982.441	8935.693	8801.348
…	…	…	…

Table S5.7: The *g* tensors of the ground $\tilde{s} = 2$ on the Fe fragments (Fe1 and Fe2).

KD		Fe1 Basis 1	Fe1 Basis 2	Fe2 Basis 1	Fe2 Basis 2
		g	*g*	*g*	*g*
1	g_X	2.21416	2.21985	2.03606	2.17165
	g_Y	2.12954	2.13481	2.10218	2.10594
	g_Z	2.02181	2.02237	2.17857	2.03905

Table S5.8: The *g* tensors of the ground Ising doublet $\tilde{s} = 1/2$ on the Fe fragments (Fe1 and Fe2) (g_X = g_Y = 0).

KD		Fe1 Basis 1	Fe1 Basis 2	Fe2 Basis 1	Fe2 Basis 2
		g_Z	g_Z	g_Z	g_Z
1	g_X				
	g_Y	8.46187	8.47359	8.17101	8.01302
	g_Z				

Estimation of the exchange interactions in FeDyFe compound by BS-DFT calculation

The calculations were carried out on the experimental geometry, by substituting computationally the Dy with Gd. This substitution is necessary in order to avoid the near-degenerate ground state of the Dy^{III} ion (it is known that DFT methods are not appropriate for description of near-degenerate ground states). We have employed ORCA program package for these calculations [1].
Computational details: B3LYP functional, SVP basis sets on all atoms, VeryTightSCF convergence thresholds, Grid5.

Further, the obtained energies of the high-spin state, and of the three low-spin states, corresponding to spin flip of one metal site, were used for the estimation of the exchange coupling constants. General equations derived from the [2] were employed for this case.

The obtained exchange parameters corresponding to Gd-Fe, were re-scaled for the interacting pair of Dy-Fe, by using the rescaling factor 7/5 (the spin of Gd) / (the spin of Dy). This approach was successfully used in [3] and [4].

Estimation of the exchange interactions in FeDyFe compound

Localization of the magnetic orbitals observed in transition metal complexes and networks [5] is even more pronounced in lanthanide-containing mono- and polynuclear compounds. This fact allows treating electronic and magnetic structure of polynuclear compounds in a two-step procedure. In the first step, reasonable fragmentation of the cluster into mononuclear fragments is performed and reliable ab initio calculations for each fragment are done. In the second step, the magnetic interaction between the fragments is introduced in an effective way. The exchange interaction between magnetic centers is considered within the Lines model [5], while the account of the dipole-dipole magnetic coupling is treated exactly. The Lines model [6] is an approximation allowing describing the anisotropic exchange interaction between magnetic sites via a single parameter. To this end, an isotropic Heisenberg model involving the true spins of the two centers is introduced with an effective parameter (the Lines exchange parameter). In a second step the matrix of this model is constructed in the basis of products of localized lowest states of the two centers obtained in fragment ab initio calculations of corresponding centers with spin-orbit coupling included. The obtained exchange matrix describes exactly the anisotropic exchange interaction in two limiting cases:

1) of two strongly axial doublets on the two sites (the case of extreme magnetic anisotropy)
2) of isotropic spins on the two sites (lack of magnetic anisotropy)
The Lines approximation is expected to be quite accurate for the description of the exchange interaction between a strongly axial doublet and an arbitrary isotropic spin. For all other cases, the Lines model [6] is a reasonable approximation. Efficient implementation of the Lines model was done in the program POLY_ANISO.

For this particular case, the employed exchange Hamiltonian is:

$$\hat{H}_{exch} = -J^{total}_{Dy-Fe_1}\hat{\tilde{s}}_{Dy}\hat{\tilde{s}}_{Fe_1} - J^{total}_{Dy-Fe_2}\hat{\tilde{s}}_{Dy}\hat{\tilde{s}}_{Fe_2} - J^{total}_{Fe_1-Fe_2}\hat{\tilde{s}}_{Fe_1}\hat{\tilde{s}}_{Fe_2} \qquad (1)$$

where $J^{total}_{Dy-Fe_1}$, $J^{total}_{Dy-Fe_2}$ and $J^{total}_{Fe_1-Fe_2}$ are parameters of the total magnetic interaction (exchange and dipolar) between corresponding metal sites ($J^{total} = J^{dipolar} + J^{exchange}$), $\hat{\tilde{s}}_{Dy} = \pm 1/2$ is the ground pseudospin on the Dy site; $\hat{\tilde{s}}_{Fe} = 2$ is the pseudospin of the corresponding Fe site.

The dipolar magnetic coupling is computed exactly, while the exchange parameters are fitted (from comparison of computed and measured magnetic susceptibility and molar magnetization). Best-fitted values are given in Table 1.

Table S5.9: Energies (cm^{-1}) and *g* tensors of the lowest 8 Kramers doublets on local Dy^{III}. The low-lying exchange doublets arising from the interactions between Dy^{III}-Fe^{II} and Fe^{II}-Fe^{II} in 2 using the magnetic couplings provided in Table 1 and the corresponding g_Z values for each doublet ($g_{X,Y} < 10^{-5}$ for all).

the lowest Kramers doublets on Dy^{III} site		low-lying exchange spectrum ($J = J_{ex} + J_{dip}$)		
KD	*E* (g_X, g_Y, g_Z)	KD	*parameters obtained from BS-DFT* *E* (g_Z)	*fitted parameters* *E* (g_Z)
1	0.0 (0.00, 0.00, 19.86)	1	0.0 (30.27)	0.0 (25.89)
2	313.9 (0.53, 3.40, 14.59)	2	3.8 (24.13)	3.1 (22.95)
3	320.9 (0.58, 3.30, 12.38)	3	5.9 (19.76)	3.8 (16.11)
4	430.1 (1.49, 2.05, 15.69)	4	8.8 (26.50)	6.9 (15.83)
5	485.4 (8.34, 7.34, 5.36)	5	10.9 (12.90)	8.5 (24.90)
6	529.4 (1.02, 2.06, 13.25)	6	15.5 (14.40)	12.2 (15.80)
7	610.9 (0.14, 1.58, 15.92)	7	18.2 (24.85)	17.1 (20.39)
8	639.5 (0.59, 1.25, 18.24)	8	22.2 (25.88)	20.2 (19.62)
		9	22.5 (21.31)	22.6 (23.56)
		10	24.0 (25.04)	23.1 (27.53)
		11	27.3 (19.87)	25.5 (20.13)
		12	29.1 (20.53)	26.4 (13.30)
		13	30.5 (10.35)	26.7 (18.99)
		14	35.1 (27.50)	34.7 (22.13)
		15	38.6 (22.63)	36.6 (18.55)
		16	39.6 (21.45)	37.8 (21.91)
		17	40.8 (24.25)	39.6 (18.03)
		18	42.4 (17.18)	39.7 (17.91)
		19	42.9 (14.33)	40.1 (22.88)
		20	44.3 (23.41)	43.1 (22.04)
		21	47.9 (17.02)	45.0 (18.20)
		22	58.4 (26.59)	57.3 (22.72)
		23	58.9 (19.81)	57.6 (20.68)
		24	60.7 (20.09)	59.0 (17.57)
		25	63.6 (17.72)	59.8 (20.53)
		26	315.4 (23.47)	313.7 (22.01)

[1] ORCA-An Ab Initio, DFT and Semiempirical electronic structure package. http://www.cec.mpg.de/forschung/molekulare-theorie-und-spektroskopie/orca.html
[2] M. Shoji, K. Koizumi, Y. Kitagawa, T. Kawakami, S. Yamanaka, M. Okumura, K. Yamaguchi, *Chem. Phys. Lett.* **2006**, *432*, 343-347.
[3] V. Vieru, L. Ungur, L. F. Chibotaru, *J. Phys. Chem. Lett.* **2013**, *4*, 3565–3569.

[4] S. K. Langley, D. P. Wielechowski, V. Vieru, N. F. Chilton, B. Moubaraki, B. F. Abrahams, L. F. Chibotaru, K. S. Murray, *Angew. Chem. Int. Ed.* **2013**, *52*, 12014-12019.
[5] P.W. Anderson *Phys. Rev.*, **1959**, *115*, 2–13.
[6] M. Lines, *J. Chem. Phys.*,**1971**, *55*, 2977.